In-situ gas analysis during the growth of hexagonal boron nitride from ammonia borane

Grace E. Wood, Zachary P.L. Laker, Alexander J. Marsden, Gavin R. Bell

Department of Physics, University of Warwick, Coventry, UK, CV4 7AL

Neil R. Wilson

Department of Physics, University of Warwick, Coventry, UK, CV4 7AL

E-mail: Neil.Wilson@warwick.ac.uk

Abstract. Ammonia borane (NH_3:BH_3) is commonly used as a stoichiometric source of nitrogen and boron for the growth of hexagonal boron nitride (h-BN) by chemical vapour deposition (CVD). We use in-situ gas analysis by mass spectrometry to investigate the active chemical components that evolve when an ammonia borane source is heated, and study how these components change after flowing through the CVD growth furnace. This also gives insight into the catalytic effect of copper substrates used for CVD growth of h-BN. We find that in vacuum, even at 40 °C, gaseous amino borane and polyaminoborane fragments are evolved from the solid source; as the temperature of the ammonia borane source increases, the amount of all components increases but proportionally more of the higher mass components are present. Gas phase reactions change the gas composition after flowing through the CVD growth furnace, depending on the temperature of the growth furnace, with increased dehydrogenation at higher furnace temperatures. Further reactions are catalysed by the copper substrate, with decomposition of the higher mass components evident at furnace temperatures > 900 °C. Direct comparison with CVD h-BN growth suggests that the lower mass components produced by lower ammonia borane source temperatures are preferred for larger island sizes and that furnace temperatures higher than 900 °C are required in order to initiate the catalytic effects of the copper substrate. In-situ gas analysis thus gives new insight into the CVD growth of h-BN, and similar methodology could be used to optimise and understand the growth of other two dimensional materials.

1. Introduction

Hexagonal boron nitride, *h*-BN, has played an important role in the rising interest in two dimensional materials (2DM) and two dimensional heterostructures (2D-HS) [1]. Although it is rarely the active element, it has found use in thin-film, few-layer or monolayer form as, amongst other things: a dielectric for improved transport properties in 2D field effect transistors [2, 3]; an atomically thin barrier for tunnelling transistors [4] and magnetic tunnel junctions [5]; an encapsulating layer for passivating air sensitive materials [6]; and in its own right as a material of potential interest for quantum optics [7]. With these myriad of exciting applications, unsurprisingly, there is increasing interest in the growth of monolayer and thin film *h*-BN. Following its successful application to the growth of graphene [8], chemical vapour deposition (CVD) of *h*-BN on transition metal substrates is proving to be an attractive option, either at low pressure (LP-CVD) or under ambient conditions [9]. However, the choice of feedstock gas is more complicated for *h*-BN than for graphene: there are only a limited number of non-corrosive, stable, stoichiometric, molecular, vapour BN sources. The two most commonly used feedstocks are borazine (the cyclical, benzene-like $B_3N_3H_6$) [10, 11, 12, 13, 14, 15, 16] and ammonia-borane (NH_3:BH_3) [17, 18, 19, 20, 21, 22, 23, 24, 25, 26, 27]. Borazine is a liquid at room temperature with a high vapour pressure, providing a convenient source for LP-CVD. As a result, it was the feedstock of choice for early surface science studies of monolayer *h*-BN [28, 29]; but it is hazardous, unstable and expensive. By contrast, ammonia-borane is cheap and comparatively safe to use; it is a solid at room temperature and is heated to produce the gaseous feedstock for CVD, but its activity for *h*-BN growth is less well understood.

Ammonia borane was widely studied as a potential hydrogen storage compound [30]: mass spectrometry investigations showed that when heated ammonia borane pyrolyses to boron nitride through polymerisation and dehydrogenation, giving off borazine when heated to above 130 °C [31]. Following this, there is confusion in the current literature as to what species evolve from heating ammonia borane and which are actively involved in the *h*-BN growth process. For CVD, the ammonia borane source is typically heated to between 60 and 130 °C, and it is often claimed that the active species is borazine [19, 22, 23, 24, 26]. Understanding what the actual gas composition is, how this changes with both source temperature and growth temperature, and how the gas composition effects the growth process, will be of vital importance to further developing *h*-BN growth. Here we apply in-situ mass spectrometry to gain insight into the evolved gas composition during the heating of ammonia borane, and how the composition changes during the low-pressure CVD (LP-CVD) growth process.

2. Experimental Methods

LP-CVD of h-BN. Following our previous methodology [25], copper foils (99.5% purity, 0.025 mm thick, Alfa Aesar 46365) were electropolished prior to growth (10 s at 5 V,

$\sim$ 1.5 A, in orthophosphoric acid and urea) and cleaned by rinsing in acetone and isopropanol. As shown schematically in Figure 1, the ammonia borane source, typically 15 mg of ammonia borane (97% purity, Sigma Aldrich 682098) in a quartz boat, was located in a side chamber with independent heating control, upstream of the growth furnace and separated by a valve. The ammonia borane temperature was measured using a thermocouple in close contact with the source boat support. The copper foils were loaded into the centre of the LP-CVD growth furnace, heated to typically 1000 °C, and annealed for 10 minutes prior to growth. After annealing, the valve to the ammonia borane source was opened to start the growth process. A flow of 10 standard cubic centimeters (sccm) of hydrogen (99.9995 %) was maintained during heating and annealing but no hydrogen was flowed during growth. After growth, the furnace was cooled to < 200 °C under hydrogen flow, and then the copper foils were removed for analysis.

SEM. A Zeiss Supra 55-VP FEGSEM was used to characterise the samples, with an accelerating voltage of 10 kV and an Inlens detector.

Mass spectrometry. As shown in Figure 1, the exhaust end of the CVD furnace was connected via a T-piece and valve to a small turbomolecular-pumped vacuum chamber equipped with standard ionization gauge and quadrupole mass spectrometer (QMS). The QMS (Mass Analyst, VSW Ltd., UK) has a range of 200 atomic mass units (amu) and can measure in a pressure range 10^{-9} Pa to 10^{-3} Pa. By adjusting the intervening valve and the sensitivity of the QMS, a wide range of absolute partial pressures could be measured without significant errors arising from residual gases. To study source sublimation and CVD growth with time resolution, a mass range of 100 amu was chosen (strictly, mass-to-charge ratio) and spectra were continuously acquired during heating. The mass spectrometer ionizes molecules and identifies the resultant ions by their mass-to-charge ratio. For the small molecules studied here we expect, for the most part, singly charged ions: this is assumed in the following analysis and hence we refer directly to the mass of the molecular species. Data are shown as 2D plots with mass on the horizontal axis and temperature on the vertical scale; the colour scale represents partial pressure.

3. Results and discussions

3.1. Gas evolution from ammonia borane

To determine the composition of the gases involved in growth, a mass spectrometer was attached downstream at the end of the LP-CVD furnace, as shown schematically in Figure 1.

First we consider the gases evolved as the ammonia borane source is heated. Figure 2 a) shows a typical spectrum produced from ammonia borane at source temperature $T_{AB} = 60$ °C. The most intense peaks correspond to 1 and 2 atomic mass units (amu), and 17 and 18 amu. The primary effect of heating ammonia borane is its dehydrogenation [31], hence the largest component of the gas produced is hydrogen,

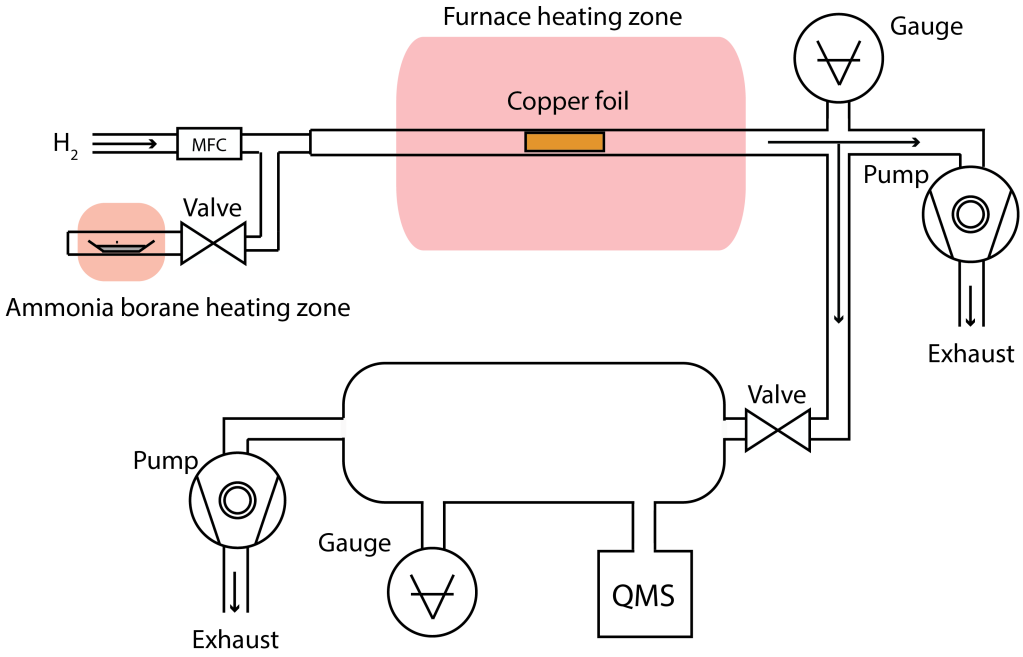

Figure 1. Schematic of LP-CVD setup with ammonia borane source separated from the main chamber by a valve, and quadrupole mass spectrometer (QMS) on the downstream end of the furnace.

amu 2. Note that the atomic hydrogen signal (1 amu) primarily arises in the electron-impact ionisation ion source of the QMS and most likely does not reflect the partial pressure in the CVD furnace. The peaks at 17 and 18 amu (mainly OH and H_2O) are much larger than the background partial pressure due to water vapour in the (unbaked) vacuum system and are due to water adsorbed in the ammonia borane powder prior to insertion in the CVD system. Although the source material was stored in a vacuum desiccator prior to use, ammonia borane is very hygroscopic and releases water vapour on heating. It is not clear what effect this water vapour may have on the *h*-BN growth process, but these results indicate that great care should be taken over the storage and handling of ammonia borane before use. In the following discussion we do not attempt a detailed quantification of the gas composition and concentrate instead on identifying the main components and their relative changes during source heating and CVD growth.

Clusters of higher mass peaks are also observed in the gas evolved from the ammonia borane powder, predominately in roughly equidistant groups at 12-16 amu, 25-30 amu, 38-44 amu, 53-57 amu, 66-72 amu, 75-85 amu and 91-97 amu. Possible molecular compositions are suggested in Table 1. To understand the origin of these peaks, we note that ammonia borane is a complex of sub-units of NH_3 (17 amu) and BH_3 (14 amu for the predominant ^{11}B isotope). The groups of peaks can thus be assigned to multiples of these sub-units, with varying number of hydrogen atoms due to fragmentation in the QMS ion source and by transformation from ammonia borane to molecular amino borane, or small fragments of polyaminoboranes (PAB)/polyiminoboranes. Interestingly, the

cluster of peaks at around 41 amu which correspond to species such as diamino borane BN_2H_5 'trimers' are of similar intensity to those at around 28 amu. The spectrum thus shows that at 60 °C the evolved gas contains monomers, dimers, trimers and small polymeric fragments of the NH_{3-x} and BH_{3-y} sub-units. The small peak at 81 amu can be assigned to the cyclical borazine, $(BN)_3H_6$, which is present at very low partial pressure: at $T_{AB} = 60$ °C, borazine makes up $\ll 1\%$ of the gas composition.

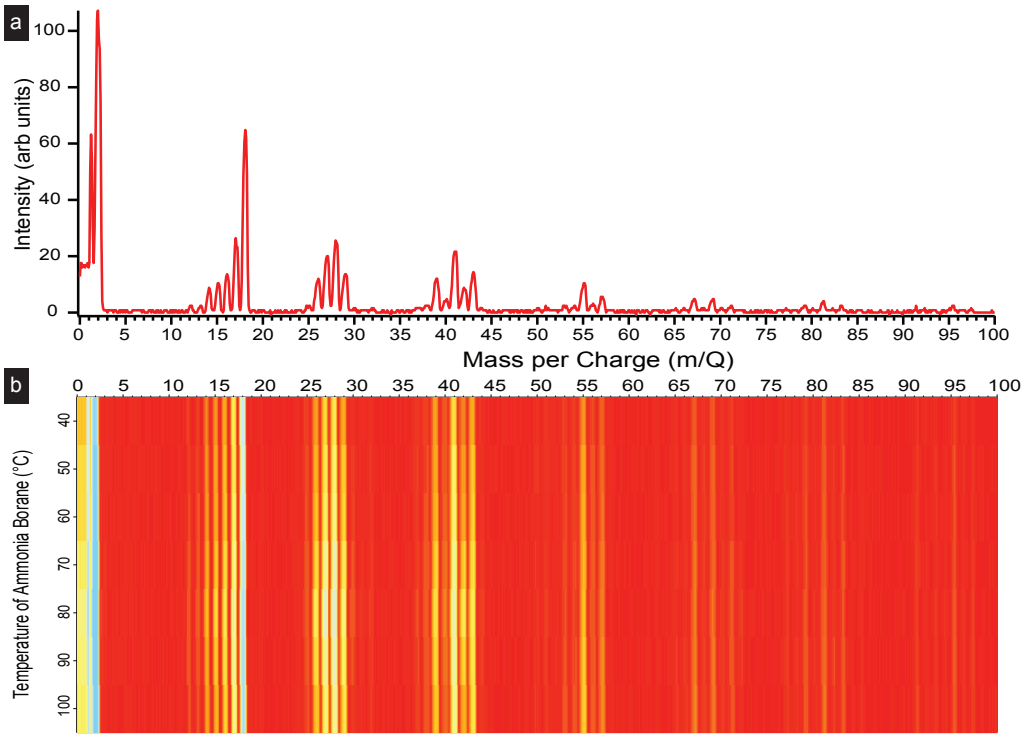

Figure 2. Above: typical mass spectrum of ammonia borane heated to the standard growth temperature of 60 °C. Below: mass spectra of ammonia borane heated from $T_{AB} = 40$ °C to 100 °C with data taken at intervals of 10 °C.

We next study how the gas composition changes with source temperature; Figure 2 shows mass spectra as the temperature of the ammonia borane source material is increased from $T_{AB} = 40$ °C to 100 °C. Note that at temperatures above 100 °C the ammonia borane was found to melt, coating the chamber in a white layer. The key features of the spectra - the presence of H_2, H_2O and PAB fragments - are prominent at all temperatures, but there are subtle changes. The amount of all components increases with temperature, as expected since the molecular vapour pressure will increase with temperature, but the higher amu clusters increase more quickly. The borazine peak at 81 amu increases gradually with temperature, but even at 100 °C is still only a very small fraction of the evolved gas. Significant quantities of ammonia borane, amino borane and PAB are present even at $T_{AB} = 40$ °C, consistent with previous measurements of the room temperature vapour pressure of ammonia borane being $\sim 10^{-4}$ Torr [32]. Finally, we note that although the ammonia borane source material contains stoichiometric

Molecules	Mass (amu)
C, BH	12
BH_2	13
BH_3	14
NH,	15
NH_2	16
OH, NH_2	17
H_2O	18
BNH	**26**
BHNH	**27**
CO, N_2, **BH_2NH, $BHNH_2$**	**28**
BH_2NH_2	**29** - amino borane
BH_3NH_2, BH_2NH_3	30
BH_3NH_3	31 - ammonia borane (borazane)
B_2NH_3	39
BN_2H, B_2NH_4	40
BH_2NHBH_2, BN_2H_2	**41**
BN_2H_3	42
BN_2H_4	43
NH_2BHNH_2	44 - diaminoborane
$B_2N_2H_3$	53
$B_2N_2H_4$	54
$B_2N_2H_5$	55
$BH_2NHBHNH_2$	56 - polyaminoborane
$B_2N_2H_7$	57
$BH_2NHBHNHBH_2$	67 - polyaminoborane
$B_3N_2H_9$	69
$B_3N_3H_6$	81 - borazine

Table 1. Masses of the likely molecular species / molecular fragments, as deduced from the mass spectrometry measurements by assuming singly charged ions. Selected intense peaks, and their likely assignments, are highlighted in bold.

quantities of boron and nitrogen, this is not necessarily the case for all components of the evolved gas as there are clearly monomers NH_{3-x}, BH_{3-y} and trimers such as BN_2H_5 present.

3.2. Gas composition changes with furnace temperature

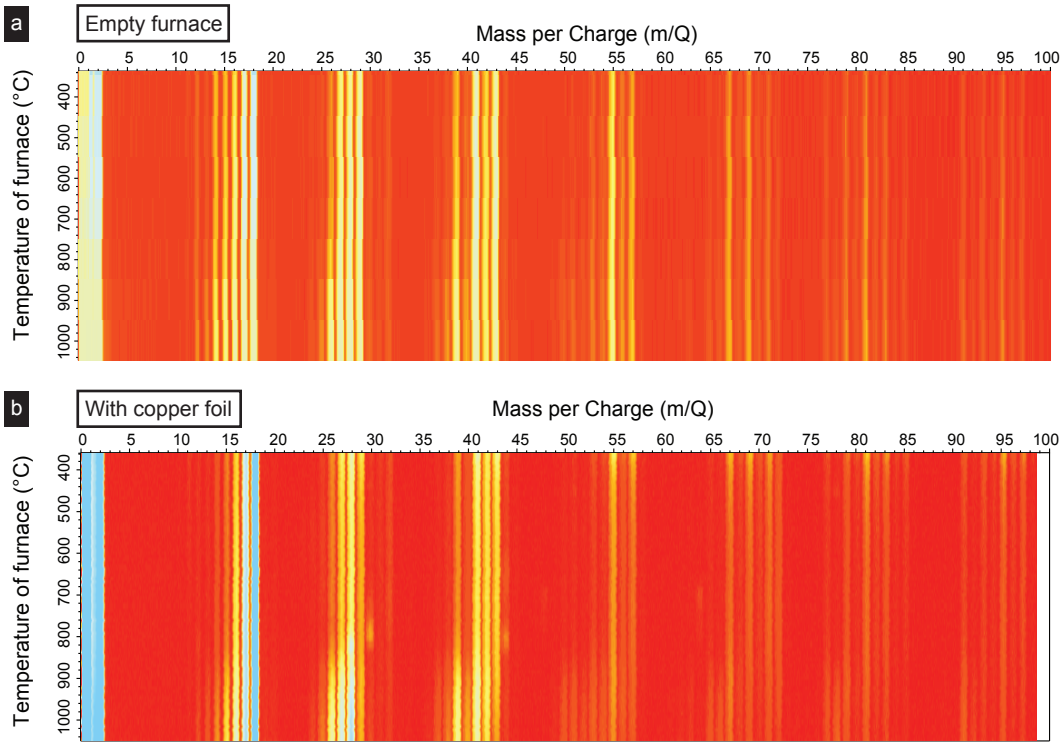

Figure 3. Mass spectra of the gas composition after flowing through the growth furnace, for fixed ammonia borane source temperature of 60 °C, whilst the furnace was heated from 100 °C to 1000 °C. Above, a); empty furnace. Below, b); with copper foil growth substrate.

Both kinetics and thermodynamics can be important for CVD growth, and at high temperatures the thermodynamic equilibrium gas compositions can be very different from the starting gas compositions. For example, during graphene growth the equilibrium gas compositions have been predicted to change significantly with temperature [33]: even if only methane and hydrogen are injected into the CVD furnace, the gas phase equilibrium composition at 1000 °C would consist of larger hydrocarbons, with the mole fraction of acetylene predicted to exceed that of methane in some pressure ranges. However, it is not clear whether such equilibrium concentrations should be reached in the time taken for the gas to flow through the furnace. Hence it is interesting to measure changes in gas composition with furnace temperature.

Figure 3 a) shows mass spectra as the furnace was heated to $T_{furnace} = 1000\,°C$, with ammonia borane source temperature kept constant at $T_{AB} = 60\,°C$. The main features of the spectra are as described earlier, with H_2, H_2O, amino borane and small PAB fragments present with varying amounts of dehydrogenation. The changes with furnace temperature are again only subtle, suggesting that equilibrium gas compositions are not reached. However, the intensities of the clusters of higher amu

peaks proportionately increase at temperatures approaching $T_{furnace} = 1000\,^{\circ}\mathrm{C}$ which shows that gas phase reactions are taking place. The lower amu peaks in each cluster also increase at higher furnace temperatures ($T_{furnace} \geq 800\,^{\circ}\mathrm{C}$), suggesting a small increase in dehydrogenation.

In-situ mass spectrometry can be used to gain insight into catalytic effects of the growth substrate. Figures 3 a) and b) compare mass spectra for an empty furnace to the same experiment with a copper foil growth substrate present. Again the main features are as before, but this time the changes are more significant. At around $T_{furnace} = 800\,^{\circ}\mathrm{C}$, peaks at 30 and 44 amu become apparent but disappear again by $T_{furnace} = 850\,^{\circ}\mathrm{C}$. We have not been able to unambiguously identify these peaks, but speculate that they are due to the reduction of the oxide layer on the copper surface and correspond to boron oxide compounds such as $(BH_2)_2O$. The dominant effect of the copper foil is apparent from $T_{furnace} = 900\,^{\circ}\mathrm{C}$ to $1000\,^{\circ}\mathrm{C}$: here there is a marked decrease in the higher mass components (such as borazine at 81 amu) and an increase in the lower amu components of each cluster of peaks. These results were reproducible across several measurements. The changes in molecular species observed here, when compared to the results without copper present, can be attributed to molecules which have been adsorbed to the copper surface, catalytically reacted at elevated temperature, and then desorbed. This suggests that the larger mass components start to be catalytically decomposed on the copper surface at $T_{furnace} \geq 900\,^{\circ}\mathrm{C}$, alongside catalytically increased dehydrogenation reactions.

3.3. Impact of ammonia borane source temperature, and growth temperature, on h-BN growth

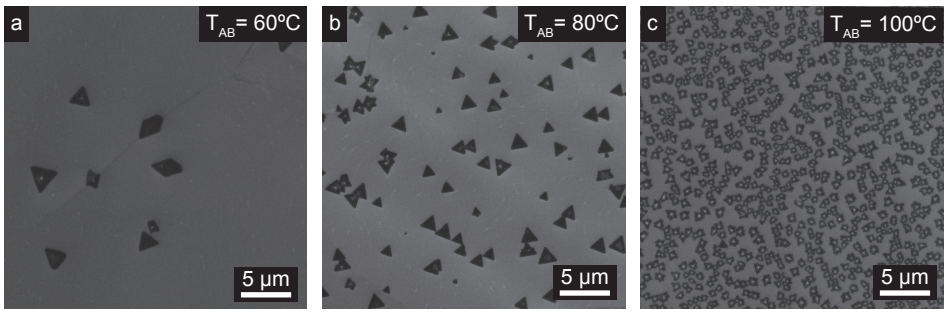

Figure 4. SEM images of h-BN growth with growth temperature $T_{gr} = 1000°\mathrm{C}$ and ammonia borane source temperature of a) $T_{AB} = 60\,^{\circ}\mathrm{C}$ (30 mg with 30 minute growth time), b) $T_{AB} = 80\,^{\circ}\mathrm{C}$ (20 mg with 5 minute growth time), c) $T_{AB} = 100\,^{\circ}\mathrm{C}$ (20 mg with 3 minute growth time).

To relate these in-situ mass-spectra to the growth of h-BN, we study the effect of ammonia borane source temperature, T_{AB}, and the furnace temperature during growth, T_{gr}, on the size, morphology and nucleation density of h-BN islands grown on copper. Figure 4 shows SEM images of h-BN growth on copper at varying temperatures of the

ammonia borane source (T_{AB} = 60 °C, 80 °C and 100 °C) at a growth temperature of T_{gr} = 1000 °C. At each temperature, predominately triangular islands are visible on the copper surface, as expected for *h*-BN under these conditions where the source flow rate is comparatively low [34], and the contrast is consistent with mainly monolayer growth [35]. However, as T_{AB} increases the nucleation density increases, the average island size decreases, and the proportion of multilayer regions (the light regions within the dark monolayer triangles [35]) increases. We can interpret these results by comparison with the mass spectrometry data: increasing T_{AB} increases the mass flow of source material and increases the mass fraction of higher amu components (trimers and small PAB fragments) which will have slower surface diffusion rates on the copper surface. Higher flux and slower diffusion of larger molecules will result in increased nucleation and smaller islands, and can also explain the increased prevalence of multi-layer regions. Although the mass spectrometry results show that the molecular species impinging on the catalyst surface are not necessarily themselves a stoichiometric source of BN, our previous investigations have shown that the composition of the resultant *h*-BN films is stoichiometrically balanced [25].

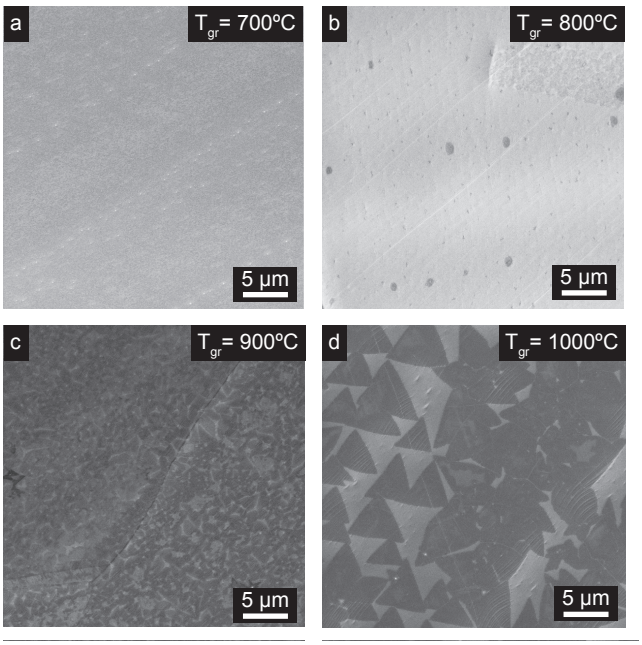

Figure 5. SEM images of *h*-BN growth with ammonia borane source temperature T_{AB} = 60 °C (15 mg with 20 minute growth time)and growth temperatures of a) T_{gr} = 700 °C, b) T_{gr} = 800 °C, c) T_{gr} = 900 °C and d) T_{gr} = 1000 °C.

The effect of changing the growth temperature (T_{gr}) whilst holding the source temperature constant (T_{AB} = 60 °C) is shown in Figure 5. The SEM images imply that *h*-BN growth only occurs for $T_{gr} \geq$ 900 °C. Since the mass spectrometry data show a sharp increase in decomposition and dehydrogenation above 900 °C with Cu foil present (Figure 3), these catalytic reactions are evidently critical to the *h*-BN growth process.

These results give insight into how growth conditions effect film quality. For most

applications, growth of high quality CVD 2DM films requires reducing the nucleation density to minimise the impact of grain boundaries, and limiting multi-layer growth to maximise uniformity. Combining the mass spectrometry results with these observations of *h*-BN island growth, this shows that lower ammonia-borane source temperatures should be used to promote large islands with low nucleation densities with high growth temperatures to activate the surface catalysed reactions.

4. Conclusions

In-situ mass spectrometry reveals that when ammonia borane is heated a complex mixture of monomers, dimers, trimers and polymeric fragments of the ammonia and borane subunits are evolved with varying amounts of dehydrogenation. The fraction of higher mass components increases with increasing source temperature. At temperatures less than 100°C the partial pressure of borazine is very low ($< 1\%$). There is evidence of gas phase reactions within the growth furnace at high temperatures and surface catalysed reactions are apparent when a copper foil is inserted in the growth furnace, with decomposition of larger molecules and increased dehydrogenation at $T_{furnace} \geq 900\,^{\circ}\mathrm{C}$. Direct correlation with LP-CVD *h*-BN growth on copper suggests that the higher mass components promote higher nucleation densities and more multilayer *h*-BN growth, with growth only becoming apparent once the surface catalysed reactions occur at $T_{gr} \geq 900\,^{\circ}\mathrm{C}$.

From these results we conclude that for *h*-BN growth from ammonia borane, the ammonia borane source should be separated from the growth chamber with independent temperature control (to limit inadvertent exposure of the substrate to feedstock before the growth step), lower source temperatures should give larger monolayer domains ($T_{AB} = 60\,^{\circ}\mathrm{C}$ gives a good compromise between source flux and gas composition) and that the catalytic role of the copper substrate is only evident at temperatures $\geq 900\,^{\circ}\mathrm{C}$. The data presented here also demonstrate that in-situ gas analysis gives new insight into the CVD growth process and can play an important role in the development of CVD for the growth of large-area high-quality 2DMs.

Acknowledgements

EPSRC is thanked for support through studentships to AJM through grant number EP/K005200/1 and ZPLL through grant number EP/M506679/1.

References

[1] Novoselov K S, Mishchenko A, Carvalho A, Neto A H C and Road O 2016 2D materials and van der Waals heterostructures *Science* **353** aac9439

[2] Mayorov A S *et al.* 2011 Micrometer-Scale Ballistic Transport in Encapsulated Graphene at Room Temperature *Nano Letters* **11** 2396–2399

[3] Kretinin A V *et al.* 2014 Electronic Properties of Graphene Encapsulated with Different Two-Dimensional Atomic Crystals *Nano Letters* **14** 3270–3276
[4] Britnell L *et al.* 2012 Field-Effect Tunneling Transistor Based on Vertical Graphene Heterostructures *Science* **335** 947–950
[5] Piquemal-Banci M *et al.* 2016 Magnetic tunnel junctions with monolayer hexagonal boron nitride tunnel barriers *Applied Physics Letters* **108** 10–13
[6] Cao Y *et al.* 2015 Quality Heterostructures from Two-Dimensional Crystals Unstable in Air by Their Assembly in Inert Atmosphere *Nano Letters* **15** 4914–4921
[7] Tran T T, Bray K, Ford M J, Toth M and Aharonovich I 2015 Quantum Emission From Hexagonal Boron Nitride Monolayers *Nature Nanotechnology* **11** 37–41
[8] Li X, Colombo L and Ruoff R S 2016 Synthesis of Graphene Films on Copper Foils by Chemical Vapor Deposition *Advanced Materials* **28** 6247–6252
[9] Yin J, Jidong L, Hang Y, Jin Y, Tai G, Xuemei L, Zhang Z and Guo W 2016 Boron Nitride Nanostructures: Fabrication, Functionalization and Applications *Small* **12** 2942–2968
[10] Shi Y *et al.* 2010 Synthesis of few-layer hexagonal boron nitride thin film by chemical vapor deposition *Nano Letters* **10** 4134–4139
[11] Kim K K, Hsu A, Jia X, Kim S M, Shi Y, Dresselhaus M, Palacios T and Kong J 2012 Synthesis and Characterization of Hexagonal Boron Nitride Film as a Dielectric Layer for Graphene Devices *ACS Nano* **6** 8583–8590
[12] Park J H *et al.* 2014 Large-Area Monolayer Hexagonal Boron Nitride on Pt Foil *ACS Nano* **8** 8520–8528
[13] Kidambi P R, Blume R, Kling J, Wagner J B, Baehtz C, Weatherup R S, Schloegl R, Bayer B C and Hofmann S 2014 In situ observations during chemical vapor deposition of hexagonal boron nitride on polycrystalline copper *Chemistry of Materials* **26** 6380–6392
[14] Kim S M *et al.* 2015 Synthesis of large-area multilayer hexagonal boron nitride for high material performance. *Nature communications* **6** 8662
[15] Caneva S, Weatherup R S, Bayer B C, Brennan B, Spencer S J, Mingard K, Cabrero-Vilatela A, Baehtz C, Pollard A J and Hofmann S 2015 Nucleation control for large, single crystalline domains of monolayer hexagonal boron nitride via Si-doped Fe catalysts *Nano Letters* **15** 1867–1875
[16] Caneva S *et al.* 2016 Controlling Catalyst Bulk Reservoir Effects for Monolayer Hexagonal Boron Nitride CVD *Nano Letters* **16** 1250–1261
[17] Song L *et al.* 2010 Large scale growth and characterization of atomic hexagonal boron nitride layers *Nano Letters* **10** 3209–3215
[18] Kim K K *et al.* 2012 Synthesis of Monolayer Hexagonal Boron Nitride on Cu Foil Using Chemical Vapor Deposition *Nano Letters* **12** 161–166
[19] Lee K H, Shin H J, Lee J, Lee I Y, Kim G H, Choi J Y and Kim S W 2012 Large-Scale Synthesis of High-Quality Hexagonal Boron Nitride Nanosheets for Large-Area Graphene Electronics *Nano Letters* **12** 714–718
[20] Kim G, Jang A R, Jeong H Y, Lee Z, Kang D J and Shin H S 2013 Growth of high-crystalline, single-layer hexagonal boron nitride on recyclable platinum foil *Nano Letters* **13** 1834–1839
[21] Gao Y, Ren W, Ma T, Liu Z, Zhang Y, Liu W B, Ma L P, Ma X and Cheng H M 2013 Repeated and controlled growth of monolayer, bilayer and few-layer hexagonal boron nitride on Pt foils *ACS Nano* **7** 5199–5206
[22] Tay R Y, Griep M H, Mallick G, Tsang S H, Singh R S, Tumlin T, Teo E H T and Karna S P 2014 Growth of large single-crystalline two-dimensional boron nitride hexagons on electropolished copper *Nano Letters* **14** 839–846
[23] Tay R Y, Wang X, Tsang S H, Loh G C, Singh R S, Li H, Mallick G and Tong Teo E H 2014 A systematic study of the atmospheric pressure growth of large-area hexagonal crystalline boron nitride film *Journal of Materials Chemistry C* **2** 1650
[24] Han J, Lee J Y, Kwon H and Yeo J S 2014 Synthesis of wafer-scale hexagonal boron nitride

monolayers free of aminoborane nanoparticles by chemical vapor deposition *Nanotechnology* **25** 145604

[25] Wood G E, Marsden A J, Mudd J J, Walker M, Asensio M, Avila J, Chen K, Bell G R and Wilson N R 2015 van der Waals epitaxy of monolayer hexagonal boron nitride on copper foil: growth, crystallography and electronic band structure *2D Materials* **2** 025003

[26] Song X, Li Q, Ji J, Yan Z, Gu Y, Huo C, Zou Y, Zhi C and Zeng H 2016 A comprehensive investigation on CVD growth thermokinetics of h-BN white graphene *2D Materials* **035007**

[27] Koepke J C *et al.* 2016 Role of Pressure in the Growth of Hexagonal Boron Nitride Thin Films from Ammonia-Borane. *Chemistry of Materials* **28** 4169–4179

[28] Auwärter W, Kreutz T, Greber T and Osterwalder J 1999 XPD and STM investigation of hexagonal boron nitride on Ni(111) *Surface Science* **429** 229–236

[29] Corso M, Auwärter W, Muntwiler M, Tamai A, Greber T and Osterwalder J 2004 Boron nitride nanomesh. *Science (New York, N.Y.)* **303** 217–20

[30] Peng B and Chen J 2008 Ammonia borane as an efficient and lightweight hydrogen storage medium *Energy & Environmental Science* **1** 479–483

[31] Frueh S, Kellett R, Mallery C, Molter T, Willis W S, King'ondu C and Suib S L 2011 Pyrolytic decomposition of ammonia borane to boron nitride *Inorganic Chemistry* **50** 783–792

[32] Sams R L, Xantheas S S and Blake T A 2012 Vapor phase infrared spectroscopy and Ab initio fundamental anharmonic frequencies of ammonia borane *Journal of Physical Chemistry A* **116** 3124–3136

[33] Lewis A M, Derby B and Kinloch I A 2013 Influence of Gas Phase Equilibria on the Chemical Vapor Deposition of Graphene *ACS Nano* **7** 3104–3117

[34] Zhang Z, Liu Y, Yang Y and Yakobson B I 2016 Growth Mechanism and Morphology of Hexagonal Boron Nitride *Nano Letters* **16** 1398–1403

[35] Sutter P and Sutter E 2014 Thickness determination of few-layer hexagonal boron nitride films by scanning electron microscopy and Auger electron spectroscopy *APL Materials* **2** 092502